

Polyamine Colloids Cross-Linked with Phosphate Ions: Towards Understanding the Solution Phase Behavior

Santiago E. Herrera,^[a] Maximiliano L. Agazzi,^[a] M. Lorena Cortez,^[a] Waldemar A. Marmisollé,^[a] Mario Tagliacruz,^[b] and Omar Azzaroni^{*[a]}

Ionically crosslinked poly(allylamine)/phosphate (PAH/Pi) colloids consist of self-assembled nanostructures stabilized by supramolecular interactions. Under physiological conditions, these interactions should be present at high ionic strength and only in a narrow pH window to be effective as drug delivery agents. In this work we study the effect of the pH and ionic strength in the chemical behaviour of inorganic phosphate (Pi), poly(allylamine hydrochloride) (PAH) and their mixture in aqueous solution (PAH–Pi). By combination of experimental measurements and a theoretical model, we demonstrate that

the driving force that leads to the formation of colloids is the electrostatic pairing between the positively charged amino groups in PAH and negatively charged HPO_4^{2-} ions. Increasing the ionic strength of the system by addition of KCl weakens the PAH–Pi interactions and narrows the pH stability window from 4 to 1.8 pH units. In addition, a fully reversible system was obtained in which the colloids assemble and disassemble by changing the pH between 6.8 and 7.1 at high ionic strength, making them suitable for use as pH-responsive nanocarriers.

Introduction

Over the past decades, supramolecular colloids have gained much attention due to their capability to load small molecules that integrate into a crosslinked structure,^[1] which turns them suitable for carrying and releasing therapeutic drugs.^[2] To be effective, the carrier particles must fulfill several requirements, namely, they should be easy to prepare, employ a non-toxic matrix, have a high loading capacity, be stable under high ionic strength conditions and degrade at target cells.^[3] One of the challenges that modern medicine faces today is the practical application of drug delivery nanocarriers for cancer treatment in localized cells^[4] to avoid non-specific chemical damage of vital organic tissues and improve drug efficiency. Typically, cancer cells present metabolic adaptations to hypoxia and nutrient deficient environments^[5] (Warburg effect) such as high glucose levels, increased lactic acid production and elevated nutrient production.^[6] Also, an adaptive feature of most cancers is the dysregulated pH of the cells. While normal differentiated adult cells present an intracellular pH (pH_i) of 7.2 and an extracellular pH (pH_e) of 7.4, tumour cells have a higher $\text{pH}_i = 7.4$ (internal alkalisation) and a lower $\text{pH}_e = 6.7$ (external acidification). The reverse pH gradient is observed due to increased expression of plasma membrane transporters and pH homeostasis protein controllers like HCO_3^- efflux co-trans-

porters, H^+ ATPases, Na^+/H^+ exchangers and carbonic anhydrase.^[7] These physiological differences between diseased and healthy tissues can be exploited for the rational design of pH-responsive nanocarriers.

In this sense, crosslinked polyamine/salt colloids represents a promising platform for drug delivery in cancer treatment being versatile in terms of chemical components,^[8] straightforward one-step synthesis by direct mixing of reactants^[9] and ability to tune colloidal size by stoichiometry control.^[10] However, many challenges remain to be approached like long-term stability in high ionic strength conditions,^[11] drug loading capacity^[12] and external stimulus-triggered disassembly.^[13]

Crosslinked polyamine/salt colloids are formed under specific conditions, where polyamines can spontaneously self-assemble in aqueous solution by crosslinking with multivalent anions to form a complex nanostructure that remains stable in a colloidal suspension.^[8a,9a,11,13a,14] Several reports indicate that the nature of the interaction between polyelectrolyte chains and salt anions is a combination of electrostatics, van der Waals forces and hydrogen bonding.^[9b,15] Besides, if the employed multivalent anion participates into acid/base equilibria, its state of charge will respond to the protonation degree, linked to the media pH. As the electrostatic interaction between ion pairs represents the major contribution to the stability of the colloid, the charge regulation plays a key role during self-assembly or disassembly.^[8a,9a,13a,14a,16]

pH-triggered particle swelling and gradual drug release at target tumor cells have been reported by Zhang et al. employing a chitosan derivative ionically crosslinked with sodium tripolyphosphate.^[19] In addition, other synthetic polyelectrolytes, such as poly(allylamine hydrochloride) (PAH), have been used as precursors for self-assembly of colloids.^[9a,18] Recently, Andreozzi et al. showed that PAH/Pi crosslinked colloids can be used as supramolecular matrixes for RNA encapsulation.^[14b] The releasing of the RNA strands was achieved by colloids

[a] Dr. S. E. Herrera, Dr. M. L. Agazzi, Dr. M. L. Cortez, Dr. W. A. Marmisollé, Dr. O. Azzaroni
Departamento de Química, Facultad de Ciencias Exactas, Universidad Nacional de La Plata, Instituto de Investigaciones Físicoquímicas Teóricas y Aplicadas (INIFTA), CONICET, La Plata 1900, Argentina
E-mail: azzaroni@inifta.unlp.edu.ar

[b] Dr. M. Tagliacruz
INQUIMAE-CONICET, Ciudad Universitaria, Pabellón 2, Ciudad Autónoma de Buenos Aires, Buenos Aires C1428EHA, Argentina

Supporting information for this article is available on the WWW under <https://doi.org/10.1002/cphc.201900046>

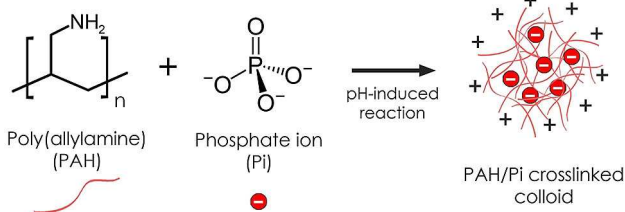
disassembling at low endosomal pH. In that work, the authors reported that the colloid suspension remained stable in a pH window between 6 and 9 and that the hydrodynamic diameter increased with increasing KCl concentration.

In the present work, we address the study of the physicochemical interactions between PAH and Pi species, varying the pH and the ionic strength of the solution. Combining experimental measurements and theoretical calculations, we show that the formation and dissolution of colloidal particles can be explained in terms of the degrees of protonation of all species in the system. We show that control of pH and salt concentration allows tuning intermolecular interactions, which in turn trigger changes in the size, charge and stability of the colloids. Understanding the solution phase behaviour of the PAH/Pi colloids allows to rationally control the physicochemical properties and directing the self-assembly process; thus, making the colloids suitable for practical applications.

Results and Discussion

Colloid Formation Without of Added KCl

We first performed preliminary experiments mixing PAH and Pi in different ratios in order to maximize the colloid suspension stability. Scheme 1 shows the formation of a PAH/Pi crosslinked



Scheme 1. Simplified PAH/Pi crosslinked colloid formation scheme.

colloid by interaction between species. When the PAH:Pi ratio was too low (excess of Pi), coalesced droplets were observed, flocculating after a few minutes. At the opposite extreme, when the PAH:Pi ratio was too high (excess of PAH), no condensation was detected. A PAH:Pi ratio of 3:1 with a PAH monomer concentration of 12 mM showed the highest stability over time, without colloid flocculation. We therefore decided to perform all further experiments with a 3:1 PAH:Pi ratio. In order to study the condensation of poly(allylamine hydrochloride) (PAH) by crosslinking with phosphate anions, 40 mL of an aqueous solution containing 12 mM of PAH (PAH) and 4 mM NaH_2PO_4 (Pi) was titrated with 30 mM NaOH. The titration process was monitored by DLS and electrophoretic measurements to determine the formation, size and Zeta potential of colloids (Figure 1a). Initially (no NaOH added), the pH of the solution was 3.40 and no formation of colloids was detected by DLS. The same behaviour was observed between pH = 3.40 and pH =

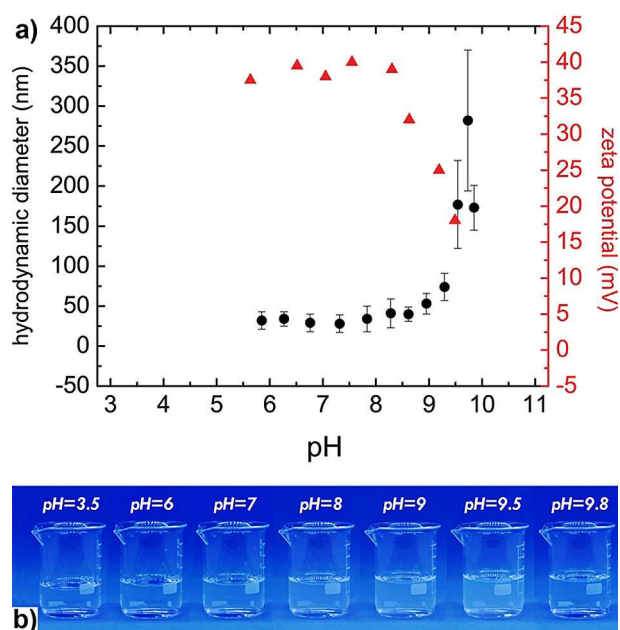


Figure 1. Colloid pH stability window without added KCl. a) Hydrodynamic diameter (black circles) and Zeta potential (red triangles) vs. solution pH for the titration of 40 mL PAH 12 mM + NaH_2PO_4 4 mM with NaOH 30 mM. b) Photographs of the solution for increasing pHs.

5.38. However, when the pH reached 5.85, a distribution of particle sizes was detected by DLS (Figure S4) with an average hydrodynamic diameter of 35 nm and a Zeta potential of +37 mV. This colloidal suspension remained stable until pH = 8.62. At this point, the Zeta potential started to decrease and the hydrodynamic diameter to increase. The inverse correlation between the size and the charge of the colloids indicates that the growing mechanism is charge-limited. Self-limiting formation and growth of monodisperse supraparticles from poly-disperse nanoparticles was studied by Kotov and co-workers.^[19] In that case, the origin of the growing limit is explained in terms of a balance between electrostatic repulsions and van der Waals attractions. The growing kinetics of the PAH/Pi crosslinked colloids could also be ruled by this balance of interactions. A series of photographs were taken at different stages of the titration process showing that the solution becomes cloudy when the pH is higher than 8 (Figure 1b). Changes in the turbidity of the solution can be attributed to both changes in size and concentration of the colloids. When the pH is low enough, a turbidity loss indicates that the sample mainly consist in free-crosslinking PAH chains. When the pH is 9.6, a maximum in turbidity indicates that most of the PAH chains in the solution are crosslinked with phosphate anions. Finally, when the pH was higher than 9.7 the colloids dissolved completely, and a translucent solution was obtained. Summarizing, DLS measurements indicated that in the absence of added KCl, the colloid stability window is between pH = 5.7 and pH = 9.7.

Figure 2 shows a TEM image of a crosslinked PAH/Pi sample prepared by mixing equal volumes of PAH 24 mM at pH = 8 and NaH_2PO_4 8 mM at pH = 8. Due to intermolecular interactions, the final pH was 9.3. A detailed description of the pH shifting by

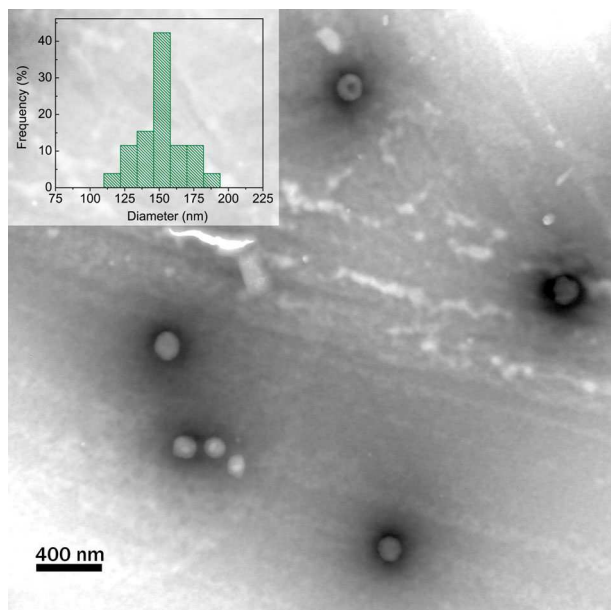


Figure 2. Transmission electron microscopy (TEM) image of crosslinked PAH/Pi colloids at pH=9.3. Inset shows a size distribution plot constructed by analysis of 12 TEM images with a total of 50 PAH/Pi particles.

the mixing process will be addressed on the following sections. A distribution of spherically shaped particles was observed with a typical diameter of 151 ± 17 nm in accordance with DLS measurements (inset in Figure 2).

The chemical composition of the crosslinked PAH/Pi colloids was studied by X-ray photoelectron spectroscopy (XPS) for different preparation pHs. For each measurement, a 3-mercaptopropylpropanesulfonic acid (MPS) modified gold slide was incubated for 24 hs in an aqueous solution containing 12 mM PAH and 4 mM Pi at the desired pH. A thin layer of colloids was obtained due to the electrostatic interaction between the negatively charged substrate and the positively charged colloids. After washing and drying the substrates, an XPS spectrum was recorded at each preparation pH. Figure 3a shows the N 1s region of the spectrum for a sample prepared at pH=8. The signals centred at 399.5 eV and 401.2 eV corresponds to nitrogen's $-NH_2$ and $-NH_3^+$ states, respectively.^[20] From the spectra analysis, the protonation degree of the polyamine in the film was determined by calculating the ratio between the protonated and the total amine peak areas. For pH=6, 7, 8 and 9, the protonation degrees were 0.70, 0.65, 0.59 and 0.57, respectively. The result shows that, inside the colloid structure, the molar ratio of $NH_3^+ : NH_2$ decreases from 5:2 at pH=6 to 3:2 at pH=9. Figure 3b shows the P 2p region of the film spectra with the typical $2p_{3/2}$ and $2p_{1/2}$ signals centred at 133.1 eV and 134.0 eV respectively, corresponding to phosphate species. The deconvolution of the N 1s and P 2p regions were compared, and the total number of nitrogen atoms per phosphorus (N/P) was calculated for each preparation pH using an XPS spectrum of $(NH_4)_3PO_4$ as reference (Figure 3c). Assuming the electroneutrality of the colloid film and knowing the protonation degree of the amine groups, the charge of the

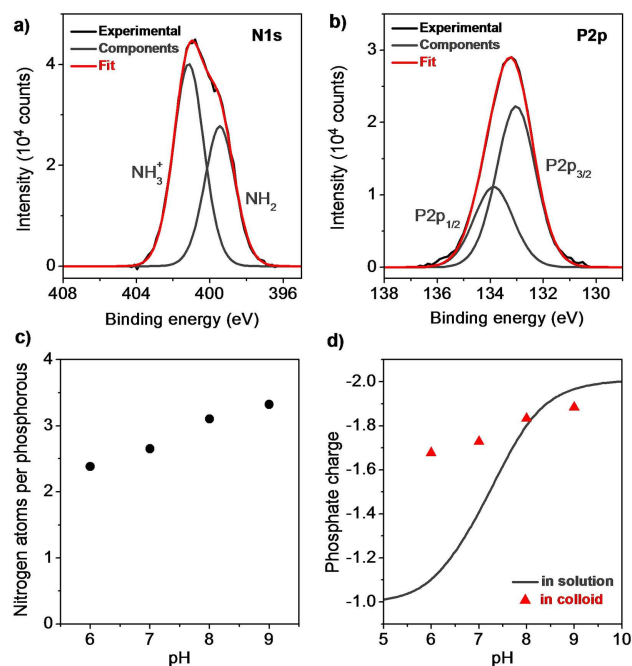


Figure 3. XPS measurements for a thin layer of PAH/Pi colloids on gold prepared at different pH. N1s (a) and P2p (b) spectra regions are depicted, indicating the corresponding experimental data (black curve), fitting (red curve) and components (grey curve) for pH=8. By quantitative analysis of the N1s and P2p regions at each pH, the number of N atoms per P (c) and the phosphate charge inside the film (d, red triangles) are plotted against pH. For comparison, the charge of phosphate species in solution is also plotted (d, grey curve).

phosphate species inside the colloid was calculated at each pH. Figure 3d shows the average charge of the phosphate species in the colloid layer (red triangles) and the corresponding value in solution obtained using the acid-base equilibrium equations for phosphate base (grey curve). The result shows that between pH=6 and pH=9 the main anionic contribution to the colloid structure comes from HPO_4^{2-} anions with a slight contribution of $H_2PO_4^-$. Even when the pH is lower than 7, the protonated amine groups are associated with HPO_4^{2-} , which shows that the driving force of the colloid formation is the coupling between charged PAH chains and HPO_4^{2-} anions. Following the same argument, Shu and Zhu showed that when phosphate is used to crosslink chitosan at pH lower than 7, the charge of the anion is too low to produce the polymer condensation.^[14a]

To examine the role of chemical interactions in the formation of the PAH/Pi colloids, the protonation equilibrium of each individual reactant was studied by potentiometric titration with NaOH 30 mM. Figure 4a shows the evolution of the pH with increasing volume of NaOH for isolated 12 mM PAH (green line) and 4 mM Pi (orange line) solutions. The titration curve for Pi in solution shows the typical buffer zone centred at pH=7.2 and a sigmoid centred at pH=9.6. The phosphate ion participates in three acid/base equilibria with pKa's of $pK_{a1}=2.12$ ($H_3PO_4/H_2PO_4^-$), $pK_{a2}=7.20$ ($H_2PO_4^-/HPO_4^{2-}$) and $pK_{a3}=12.36$ (HPO_4^{2-}/PO_4^{3-}). Figure S2 (supporting information) shows a calculated Pi speciation diagram in the evaluated pH range,

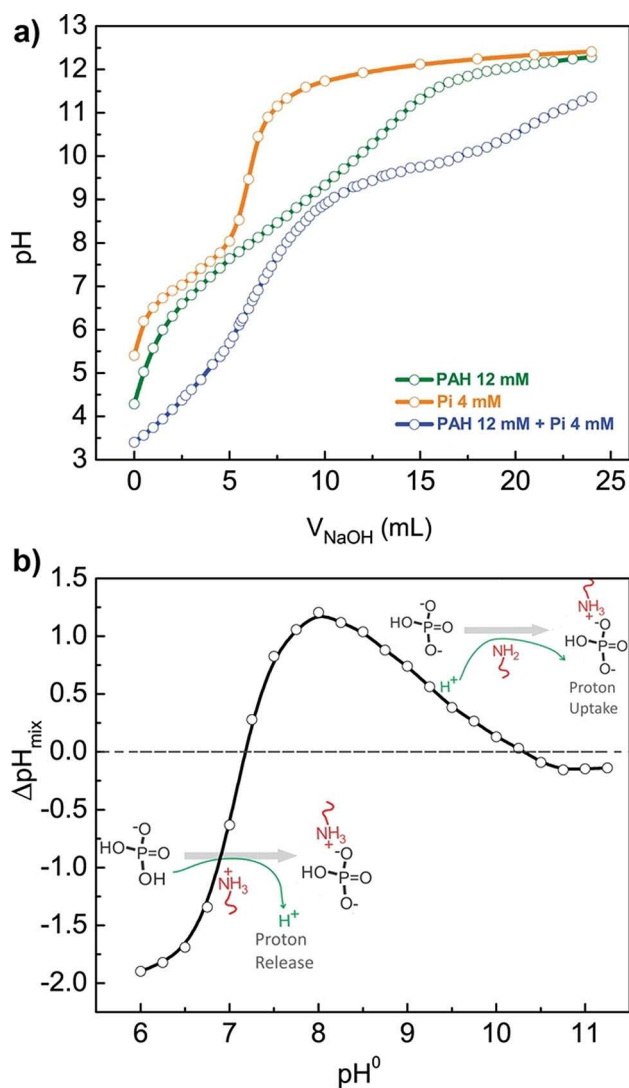


Figure 4. System pH response without added KCl. a) Potentiometric titration curves of 40 mL PAH 12 mM (green line), 40 mL NaH_2PO_4 4 mM (orange line), 40 mL PAH 12 mM + NaH_2PO_4 4 mM (blue line). The solutions were titrated with 30 mM NaOH. b) Shift of the pH due to the mixing process vs. initial pH.

obtained from the experimental titration curve. The titration curve for PAH shows a very broad transition between $\text{pH}=6$ and $\text{pH}=11.5$.^[16] Taking into account that the pK_a of a terminal primary amine group on a hydrocarbon chain is ~ 10.6 (octadecylamine), the pK_a of each amine group in a PAH chain should also be close to that value.^[21] However, the positive electrostatic environment generated by protonated amino groups hinders the protonation of adjacent amines, which decreases the protonation affinity of PAH.^[22] Moreover, since this positive electrostatic potential changes with pH (because the net charge of the amine groups changes with pH), the titration curve of PAH is much broader than an ideal titration curve (Figure 4a, green line).^[23] Rubner and co-workers reported a similar behaviour with a $\text{pK}_{a,1/2}$ (value of pH for which half of the amino groups are protonated) between 8 and 9.^[22] The protonation degrees of the PAH at different pHs were

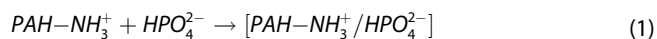
calculated from the titration curve using Equation 8 in Supporting Information. Using these protonation degrees, we constructed the speciation diagram for PAH in the evaluated pH range (Figure S1 in Supporting Information). For $\text{pH}=6, 7, 8$ and 9, we calculated protonation degrees of 0.90, 0.78, 0.62 and 0.44. Comparing this data with the equivalent obtained with XPS inside the crosslinked colloids (0.70, 0.65, 0.59 and 0.57), it can be observed that the interaction between PAH and Pi produces a partial deprotonation of PAH at pH lower than 8.5, and a partial protonation at pH higher than 8.5.

After studying the titration behaviour of the individual components, the titration of the mixture was performed. Figure 4a (blue line) shows the potentiometric titration of a mixture of 12 mM PAH + 4 mM Pi, in which a smooth increase in the pH with added NaOH followed by plateau zone centered at $\text{pH}=9.75$ are observed. Interestingly, the PAH/Pi colloids tend to grow in size and concentration below this point (Figure 1).

To study the interactions between PAH and Pi, we calculated the shift of pH caused by the mixing process ($\Delta\text{pH}_{\text{mix}}$). First, we obtained the volume V_1 of NaOH necessary to reach a given pH (which we denote pH^0) by intersection in the titration curve of Pi. Following the same procedure, a volume V_2 of NaOH was obtained using the PAH titration curve for the same pH^0 . Next, we sum V_1 and V_2 and intersect the resulting volume in the mixture titration curve in order to obtain pH_{mix} . This value is the pH that the mixture has after adding a volume of NaOH equal to $(V_1 + V_2)$. On the other hand, pH^0 is the pH that the mixture would have after adding such volume if PAH/Pi complex formation had not occurred. Moreover, the differences between these two values, $\Delta\text{pH}_{\text{mix}} = \text{pH}_{\text{mix}} - \text{pH}^0$ is equal to the pH change that is expected upon mixing Pi and PAH solutions at pH^0 (neglecting dilution effects). The values of $\Delta\text{pH}_{\text{mix}}$ were calculated for different pH^0 values, covering a range between 6 and 11, and plotted in Figure 4b against pH^0 . Therefore, this plot shows the changes in the solution pH due to interactions between phosphate species and PAH chains at a given initial $\text{pH} = \text{pH}^0$.

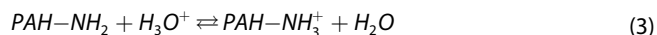
The plot in Figure 4b reveals that if pH^0 is lower than 7.17, the interaction between PAH and Pi produces a negative shift of the pH (proton release). However, if pH^0 is between 7.17 and 10.32, a positive shift is observed (proton consumption). Finally, when pH^0 is higher than 10.32 no significant change in the pH is observed, which indicates that the interactions are minimum. Interestingly, for $\text{pH}^0 = 7.17$, mixing of the reactants and complex formation does not produce any change in the solution pH. Similar results were observed by Lawrence and Lapitzky using tripolyphosphate (TPP) and pyrophosphate (PPI) as crosslinking agent varying TPP/PAH and PPI/PAH ratios starting from different parent solution pHs.^[24] In their work, when PAH is mixed either with TPP or PPI at $\text{pH}^0 > 8$, a positive shift in the pH is detected due to crosslinking. Also, when pH^0 is placed round 4.5, a negative shift in the pH is observed. These authors suggest that this effect arises from pK_a shifting toward high valence states in each specie and consequently the corresponding proton releasing or uptake from the aqueous solution.

At low pH⁰ (6 to 7.17), the negative value of $\Delta\text{pH}_{\text{mix}}$ indicates that the complex formation between the PAH chains and the Pi species produces an increment in the H⁺ concentration. As it was demonstrated in Figure 1, in this region the concentration of colloids is very small, and the PAH chains remain almost free of crosslinking. Considering the acid/base equilibria (1) and (2), the association between HPO₄²⁻ and PAH chains (Equation 1) could produce the observed increment of the H⁺ concentration by shifting the phosphate equilibria (Equation 2) towards products.



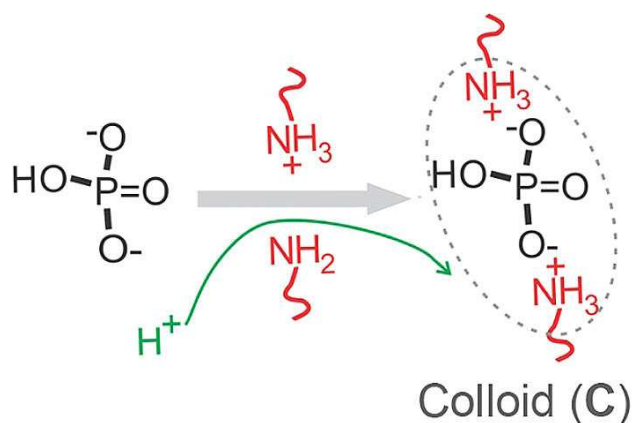
Simultaneously, the complex formation between HPO₄²⁻ anions and polyamine (eq. 1), forces the amine groups to get charged by uptake of protons from the solution as is shown in Equation 3. This phenomena was also reported by Petrov *et al.* for interpolymer complex formation of poly(allylamine hydrochloride) and poly(sodium 4-styrenesulfonate).^[16]

When the pH⁰ is higher than phosphate pKa₂, the concentration of HPO₄²⁻ is high enough and the proton uptake by PAH (eq. 3) dominates over the proton release by H₂PO₄⁻ (eq. 2). This H⁺ uptake produces the increment of the solution pH observed on Figure 4b in the range between pH⁰=7.17 and pH⁰=10.32. In this way, the strong interaction between PAH and HPO₄²⁻ clearly emerges as a hypothesis in order to interpret the results.



When all the PAH becomes saturated with HPO₄²⁻ anions, a condensation between chains is produced, which increases the colloid C concentration (Figure 1b). The protonation of the PAH and the crosslinking between chains by coupling with HPO₄²⁻ anions are summarized in Scheme 2

At high pH⁰ (>10.32), the PAH becomes neutral by total deprotonation.^[16,22,25] In these conditions, the crosslinked structure is no longer stable, and the colloids dissolve. This

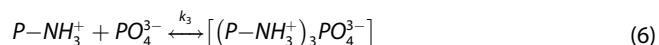
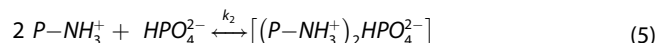
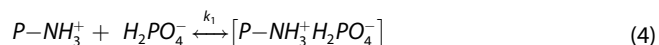


Scheme 2. Scheme of PAH/Pi crosslinking process at pH between 7.17 and 10.32.

phenomenon is consistent with the data shown in Figure 1 where there is a drop in the surface charge of the particles at high pH. The plot in Figure 4b at pH⁰ > 10.32 also agrees with the total deprotonation of the amine groups. If the polyamine is no longer charged, the interaction between the PAH chains and the Pi species becomes negligible and the $\Delta\text{pH}_{\text{mix}}$ tends to zero.

To validate the hypothesis, the pH of the PAH–Pi solution vs. V_{NaOH} was calculated analytically, using a model that considers the formation equilibrium of a complex between the protonated amine groups of the polyamine (–NH₃⁺) and Pi (see supporting information). We will consider the possibility of complexation between PAH and three different phosphate species: H₂PO₄⁻, HPO₄²⁻ and PO₄³⁻, and show that the predictions of our model are only compatible with experiments for the case where complexation occurs with HPO₄²⁻ anions.

Equations 4, 5 and 6 show the formation of neutral complexes of P–NH₃⁺ (where P denotes the polymer backbone) with H₂PO₄⁻, HPO₄²⁻ and PO₄³⁻ anions respectively. The equilibrium constants of each complex formation were named k_1 , k_2 and k_3 .



Plots in Figures 5a, b and c show the calculated titration curves for different values of k_i . As a comparison, the experimental titration curve of the PAH–Pi solution is also plotted. For $k_i=0$ (no complex formation), curves for $i=1, 2$ and 3 are, as expected, equal. These curves are also equal to the curve of pH⁰ vs. ($V_1 + V_2$) calculated from experiments because this curve, as we explained above, corresponds to the titration of non-interacting Pi and PAH (grey dash line in Figure 5). Assuming the formation of a complex between P–NH₃⁺ and H₂PO₄⁻ (Figure 5a) results in a family of curves for which the pH is always an increasing function of k_1 . Also, none of these curves matches the experimental measurement. If now the considered Pi specie is PO₄³⁻ (Figure 5c), a negative shift on the pH is observed when the volume of NaOH is lower than 10.6 ml and the curves calculated for different values of k_3 intersect at pH = 7.9 and $V_{\text{NaOH}} = 10.6$ ml. In this case, as in the previous one, the calculated curves do not match the experimental measurement for any value of k_3 .

Let us now consider the formation of a complex between the protonated amine and the divalent HPO₄²⁻ anion (Figure 5b). In this case, we observe that the calculated curves approach the experimental results for $k_2 \sim 10^6$ – 10^7 . An intersection between the calculated and the experimental curves is observed at pH = 7.14, which is exactly the same pH for which we observed zero $\Delta\text{pH}_{\text{mix}}$ in Figure 4b. This result is explained from the fact that at pH = 7.14, the formation of the complex does not change the H⁺ concentration in solution because the number of protons released by H₂PO₄⁻ to form HPO₄²⁻ is equal to that taken by P–NH₂ to form P–NH₃⁺. In principle, the value of k_2 dictates the amount of complex formed, and therefore the

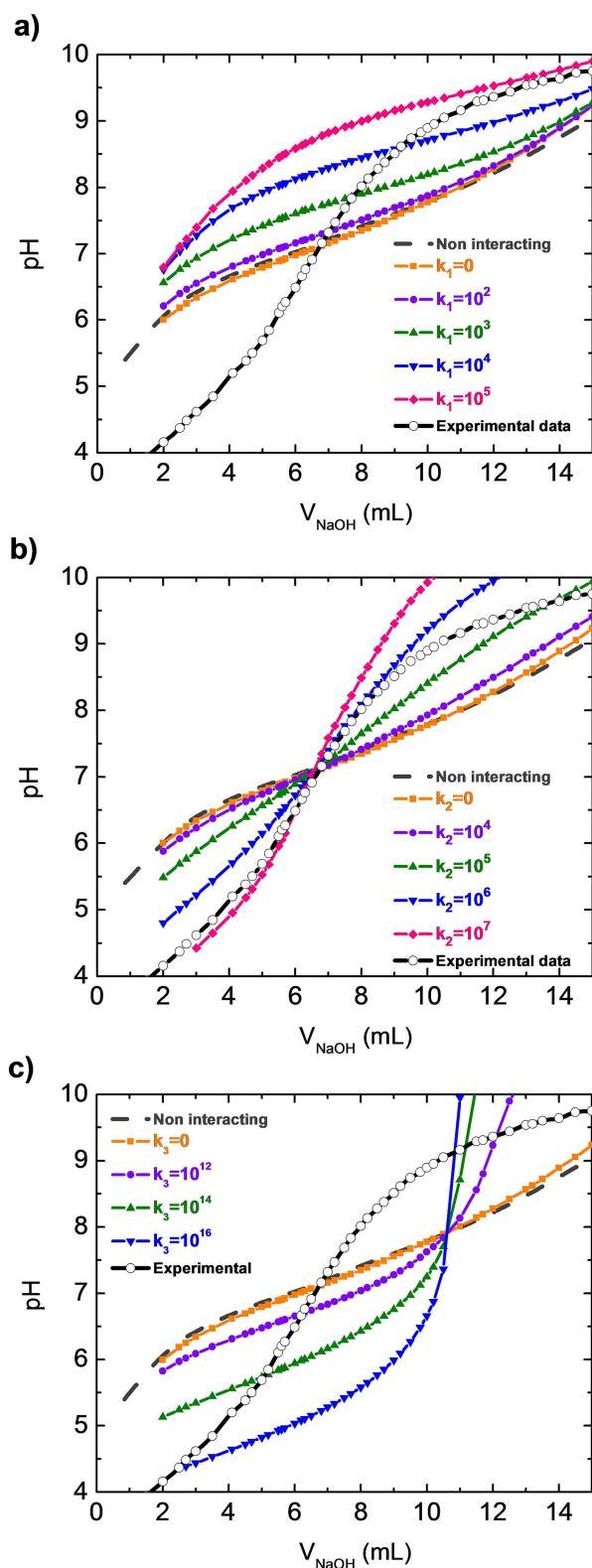


Figure 5. Calculated titration curves for a 40 mL aqueous solution of PAH 12 mM + Pi 4 mM with NaOH 30 mM considering formation of $[\text{P}-\text{NH}_3^+ \text{H}_2\text{PO}_4^-]$ (a), $[(\text{P}-\text{NH}_3^+)_2\text{HPO}_4^{2-}]$ (b) and $[(\text{P}-\text{NH}_3^+)_3 \text{PO}_4^{3-}]$ (c) complexes. Different association constants k_i were evaluated in each case. Black curves correspond to the experimental data obtained with potentiometric titration. Grey dash line represents the titration curve for the system PAH-Pi without considering interactions (pH^0 vs $(V_1 + V_2)$).

higher the value of this constant, the larger the magnitude of the change in pH upon mixing. However, since at $\text{pH}=7.14$ the complex formation does not change the concentration of protons in solution, the value of k_2 has no effect on the pH of the solution.

In few words, our theoretical model confirms that HPO_4^{2-} is the Pi specie that forms the complex with PAH and, eventually, produces the crosslinking between polymer chains leading to colloid formation. This result is in accordance with the XPS data showed in Figure 3 in which the average phosphate charge found inside the colloid structure was -2 . Furthermore, the data shows that the value of k_2 is expected to be between 10^6 and 10^7 .

At this point, we should mention that the agreement of the model with the experiments in Figure 5b is only semi-quantitative because there is no value of k_2 that perfectly fits the data in the whole range of pH. We believe that this is due to a limitation of the model, which neglects the effect of local environment on the complex formation equilibrium.

In other words, since the local environment experienced by the amine groups and Pi ions changes with pH, the apparent value of k_2 will also change. In fact, one would expect that at low pH, the presence of a large number of positively charged amine group on the PAH backbone will favour complex formation between adjacent NH_3^+ groups and Pi, in order to decrease electrostatic repulsions. Following this idea, the apparent value of k_2 should be larger at low pH than at high pH. This expectation is fully consistent with the results of Figure 5b, which shows that the theoretical model can fit the experimental results for $\text{pH} < 7.14$ using a large value of k_2 ($k_2 = 10^7$), while a smaller value ($k_2 = 10^6$) works better for $\text{pH} > 7.14$.

Colloid Formation in 0.2 M KCl

Next, the solution behaviour of the PAH/Pi colloids was studied in the presence of 0.2 M KCl. A potentiostatic titration of a 40 mL aqueous solution of 12 mM PAH + 4 mM Pi + 0.2 M KCl with 30 mM NaOH was monitored by DLS and electrophoretic mobility measurements to evaluate the hydrodynamic properties of the colloids and the stability pH window. Figure 6a shows that the formation of PAH/Pi colloids starts at a $\text{pH}=6.8$ and dissolves at $\text{pH}=8.6$ leading to a narrow stability window of 1.8 pH units in comparison with the 4 pH units stability window of the system without added salt (Figure 1). The Zeta potential of the colloids remained almost stable in $+20$ mV during the entire pH range. The fact that the Zeta potential values were lower respect to the non added salt system, can be explained in terms of the Gouy-Chapman theory which indicates that the potential drop from the surface is increased with the electrolyte concentration at constant surface charge density. The hydrodynamic diameter of the particles is higher than for the system without added salt, with an average diameter of 260 nm. Also, growth of the particles near the dissolution point is now not observed. The photographs in Figure 6b show that, in the very moment in which the colloids are formed, a fully cloudy solution is obtained in concordance

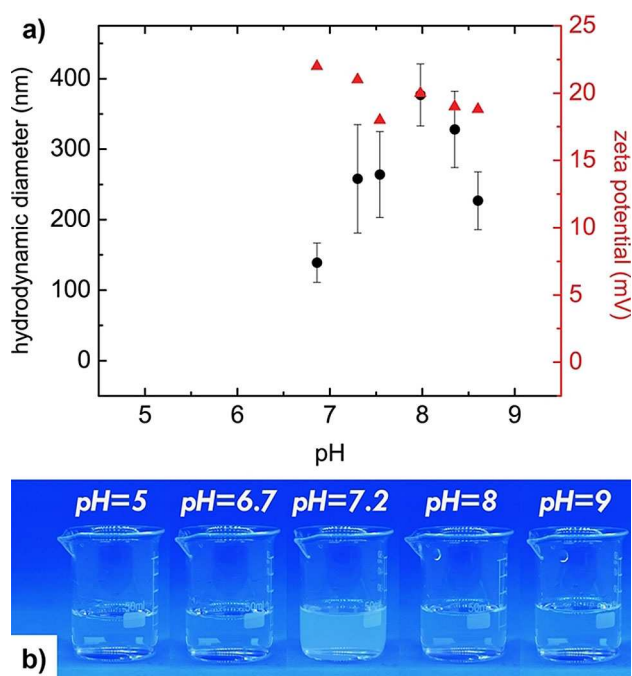


Figure 6. Colloid pH stability window with added KCl. a) Hydrodynamic diameter (black circles) and Zeta potential (red triangles) vs solution pH of 40 mL PAH 12 mM + NaH_2PO_4 4 mM + 0.2 M KCl titrated with NaOH 30 mM. b) Photographs indicating the solution fashion with increasing pH.

with a size distribution detection (increasing in colloid concentration) and an increment in particle diameter respect to the system without salt. DLS measurements on both samples (with and without salt) at pH=7.2 confirms this observation if the derived count rate is considered. For the sample without salt, the derived count rate at pH=7.2 was 6500 kcps and the analogous with salt was 85000 kcps, meaning that for the same pH, the addition of salt results in an increment of more than ten times the derived count rate.

The data presented shows that the addition of salt in an aqueous solution containing PAH/Pi crosslinked colloids can result either in the total dissolution or in an increase in their concentration and size, depending on the pH of the solution. If the pH is 6 or 9, the addition of salt tends to dissolve the colloids, while at pH=7.2, the addition of salt produces an increment in the size and concentration.

Figure 7a shows the titration curves for 4 mM Pi (orange line), 12 mM PAH (green line) and the mixture of 4 mM Pi + 12 mM PAH (blue line) with 30 mM NaOH in the presence of 0.2 M KCl. Analogously to the analysis performed for Figure 4, we evaluated the effect of the complexation between charged species by plotting the shift of the pH due to the mixing process, $\Delta\text{pH}_{\text{mix}}$, against the initial solution, pH^0 . For comparison, data without added salt was also included in the same plot. The plot in Figure 7b shows that the values of $\Delta\text{pH}_{\text{mix}}$ in the presence of added salt are much smaller than those in salt-free solutions, which indicates that the presence of KCl produces a decrease in the interaction between the protonated amine groups and HPO_4^{2-} species. Lawrence and Lapitzky have

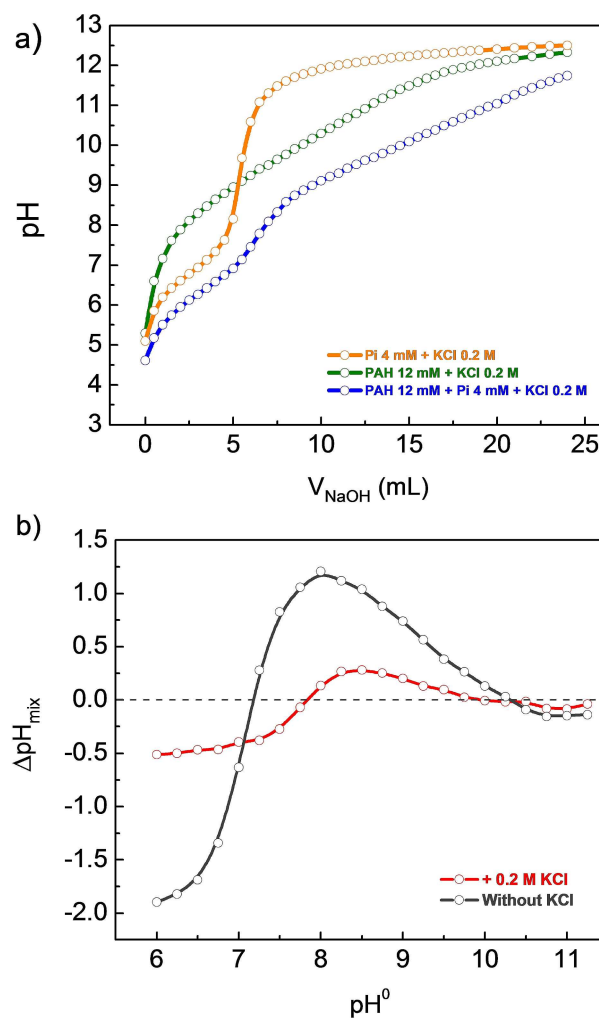


Figure 7. System pH response with added KCl. a) Potentiometric titration curves of 40 mL 12 mM PAH + 0.2 M KCl (green line), 40 mL 4 mM NaH_2PO_4 + 0.2 M KCl (orange line) and 40 mL 12 mM PAH + 4 mM NaH_2PO_4 + 0.2 M KCl (blue line) with 30 mM NaOH. b) Shift on the pH by the mixing process vs initial pH. For comparison, the system without added KCl is also shown (grey line).

arrived to similar conclusions when studying the complexation between PAH and TPP or PPI. Here, the addition of NaCl into the system led to a decrease in the pH shifting by crosslinking when $\text{pH}^0 = 7$.^[24] According to Figure 6, added salt also increases the size of the colloids. Recently, J. B. Schlenoff reviewed the effect of salt concentration on the microstructure of hydrated polyelectrolyte complexes.^[26] As the amount of salt in solution is increased, the electrostatic bonds between the positively charged (Pol^+) and the negatively charged (Pol^-) polymers begin to break, and the charged polymer units couple with salt ions. This process leads to a transition between close packed complex structures (no salt) and open coacervate structures (high salt concentration). Eventually, if the salt concentration is high enough, the polyelectrolyte complexes completely dissolve. Following the same argument, a similar conclusion can be drawn for PAH/Pi crosslinked structures, explaining the observed changes.

The effect of the chloride and potassium ions on the PAH–Pi interaction also impacts in the window of pH stability. In this case, as the amine groups are partially coupled to chloride anions, the concentration of HPO_4^{2-} in solution must be higher than in salt-free solutions in order to crosslink and collapse the PAH chains. Thus, a pH higher than in salt-free solutions will be needed to observe colloid formation. For the same reason, the deprotonation of the PAH amine groups produces the dissolution of the colloid at lower pH values than in solutions without added salt.

Figure 7b shows that the addition of salt produces a positive shift of the pH^0 at which $\Delta\text{pH}_{\text{mix}}=0$ (zero crossing point), from 7.15 to 7.82. The same behaviour was observed in the theoretically calculated titration curves with 0.2 M KCl (Figure S3), which shows that curves for different values of k_2 (formation of P- HPO_4^{2-} complex) intersect at $\text{pH}=7.63$. The pH^0 value required for $\Delta\text{pH}_{\text{mix}}=0$ changes with addition of KCl because the different protonation degree of the PAH depends on solution ionic strength (see Supporting Information).^[27]

Finally, the reversibility of the colloids formation/dissolution in physiological ionic strength (0.2 M KCl) was evaluated with DLS in a region near physiological pH (7.2). For this purpose, 40 mL of an aqueous solution of 12 mM PAH + 4 mM Pi + 0.2 M KCl was brought to $\text{pH}=6.6$ with 1 M NaOH. Then, we produced small positive and negative shifts of the solution pH by adding small aliquots of NaOH 1 M or HCl 1 M. The solutions were studied with DLS, which was used to measure the size distribution and count rate at each pH. Figure 8 shows that a

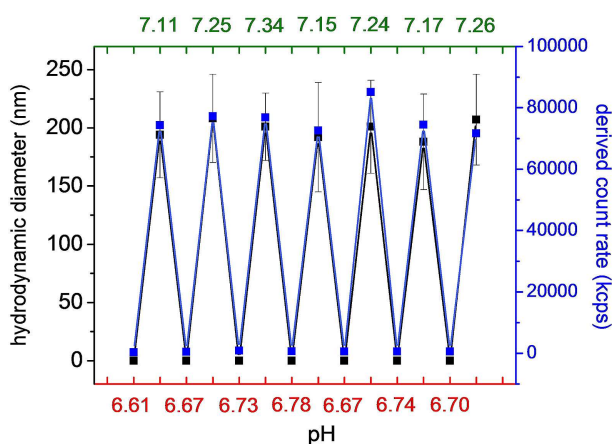


Figure 8. Dynamic light scattering hydrodynamic diameter and derived count rate of PAH/Pi crosslinked nanostructures in aqueous solution in presence of 0.2 M KCl at different consecutive pH. Colloid formation/dissolution reversibility near physiological pH.

fully reversible behaviour was observed: the system switched between colloids with an average hydrodynamic diameter of 200 nm at pH higher than 7.11 and colloid-free solution (total dissolution) at pH lower than 6.78. DLS measurements also showed a narrow particle size distribution every time the colloids were formed at pH close to 7.2 (Figure S5), which indicates that the system remains homogeneous over consec-

utive formation/dissolution cycles. Nevertheless, the same experiment carried out in a solution without added KCl, lead to a continuous increase in the salt concentration in successive cycles of HCl/NaOH addition, which produces constant changes in the colloid structure and lead to a non-reversible system.

The study of PAH/Pi colloid formation/dissolution in aqueous solution, with and without salt, can be used as tool for designing responsive nanocarriers. Knowing that the pH stability windows between both systems do not overlap (Figures 1 and 6), for low initial salt concentration, colloids can either assemble or disassemble by simply increasing KCl concentration if the $\text{pH}\sim 7.2$ or $\text{pH}\sim 9.5$ respectively. This behaviour can be used for trapping or releasing small molecules using changes in the media ionic strength (salt responsive nanocarriers). For high initial salt concentration (physiological ionic strength), colloids can also be used for trapping and releasing of small molecules, but this time the assembly/disassembly process can be triggered by small changes in the media pH around $\text{pH}\sim 7$ (pH responsive nanocarriers).

Conclusions

In this work, we assess the interactions between poly(allyl-amine) chains and phosphate species with the goal of improving our fundamental understanding of the behaviour of PAH/Pi crosslinked colloids in solution phase. Using a combination of experimental measurements and theoretical modelling, we show that the main phosphate species that is responsible for crosslinking PAH chains is the divalent HPO_4^{2-} anion. In addition, a comparison of the potentiostatic titration curves of the individual reagents and the mixture, showed that the interaction between $-\text{NH}_3^+$ and HPO_4^{2-} produces a negative shift in the solution pH when the initial pH^0 is below 7.15. This behaviour can be explained in terms of an increase in the concentration of protons due to the displacement of the phosphate acid/base equilibrium towards HPO_4^{2-} anions. When pH^0 is higher than 7.15, the crosslinking between PAH chains produces proton uptake from the solution, which increases the pH and, thus, changes the sign of $\Delta\text{pH}_{\text{mix}}$ from negative to positive. At pH^0 near 10, the colloids tend to dissolve by deprotonation of PAH amine groups. Without added salt, a wide stability pH range between 5.8 and 9.8 is observed. The concentration, size and Zeta potential of the colloids showed significant changes in the evaluated pH stability range making the preparation pH a key factor in order to design colloidal entities with functional properties.

Increasing the ionic strength by addition of KCl produced dramatic changes in the colloidal dispersion behaviour. The salt anions interfere between $-\text{NH}_3^+$ and HPO_4^{2-} , narrowing the pH stability window from 4 to 1.8 pH units. Moreover, they anions produce an increment in the average particle size and a decrease in the Zeta potential. An aqueous solution containing 12 mM PAH, 4 mM Pi and 0.2 M KCl showed, in a reproducible way, that the assembly and disassembly of the colloids can be reversibly controlled by changing the solution pH round $\text{pH}=7$.

Experimental Section

Poly(allylamine hydrochloride) (PAH) ($M_w \sim 17500$) and 3-mercaptopropylsulfonic acid sodium salt (MPA) were purchased from Sigma-Aldrich. Sodium hydroxide, hydrochloric acid and potassium chloride were purchased from Anedra. Sodium phosphate monobasic monohydrate was purchased from Cicarelli. All chemicals were used without further purification.

The pH and potentiometric titration measurements were carried out using an Adwa AD8000 pH-meter with a 0.01 units sensibility running at 20 °C, calibrated with commercial buffer solutions of pH = 4, 7 and 10. For potentiostatic titrations, 40 mL of 12 mM PAH, 4 mM Pi and a mixture of 12 mM PAH and 4 mM Pi with and without KCl 0.2 M were titrated using a NaOH 30 mM aqueous solution under continuous stirring at 50 rpm. Dynamic light scattering (DLS) and zeta potential measurements were carried out with a ZetaSizer Nano (ZEN3600, Malvern, U.K.) at 20 °C using DTS0012 and DTS1060 disposable cuvettes. For particle size measurements a 173° backscatter angle with 10 runs (20 sec/run) were used for each sample. Particle zeta potential was measured from the electrophoretic mobility with a Laser Doppler Velocimetry using a general purpose analysis model in a 100 runs experiment for each sample.

Experiments of Figures 1a and 6a were carried out in the following way: a 40 mL aqueous solution containing 12 mM PAH (monomer $M_w = 93.5$) and 4 mM Pi with (Figure 6a) and without (Figure 1a) KCl was placed in a 100 mL beaker and titrated with 30 mM NaOH using a 25 mL burette. The pH was registered during the entire experiment. For different amounts of added NaOH, a 1.3 mL aliquot of solution was placed in the DLS cuvette and particle size was analyzed. After DLS measurement, the 1.3 mL aliquot was placed back into the beaker and the titration was continued. This method was repeated until the pH reached 10.5. In a new experiment, the zeta potential was analyzed. For this, a similar method was followed but using a 1 mL aliquot of solution and discarding it after each measurement.

Theoretical prediction of titration curves: Titration curves were predicted by solving the system of coupled equations comprised by the acid-base equilibria equations and mass-balance equations for the phosphate ions and the amino/ammonium groups in PAH, the charge-balance equation including all ionic species in the system and the equilibrium equation for the formation of the phosphate-ammonium complex. In the latter equation, we explored different possible stoichiometries for the complex. The acid-base equilibrium equation for the amino/ammonium groups (dissociation fraction vs. pH) was obtained from the experimental titration curve for PAH in order to consider charge-regulation effects due to the interaction between neighbor groups.^[28] The supporting information describes the formulation of the model in detail. The set of equations to be solved does not have an analytical solution, so we solved it numerically using a purpose-written program in Octave.

The morphology of the colloids was studied by Transmission Electron Microscopy (TEM). Samples were stained with phosphotungstic acid on carbon grids to create contrast. Images were obtained with a JEOL microscope (120 kV) equipped with a Gatan US1000 CCD camera.

X-ray photoelectron spectroscopy (XPS) was performed using a SPECS SAGE HR 100 spectrometer with a Mg K α (1253.6 eV) source at 12.5 kV and 10 mA. The BE resolution for detailed spectra of the C1s, O1s, N1s, and P2p regions was 1.1 eV. Quantitative analysis of spectra was carried out with the Casa XPS 2.3. 16 PR 1.6 software. Shirley baselines and Gaussian/Lorentzian (30%) product functions were employed. The signal of aliphatic C1s was assigned to 285 eV

to discount any surface-charging effects. For the atomic ratio N/P, more precise calculations were performed by recording the XPS spectrum (NH₄)₃PO₄ (Sigma Aldrich) powder in the same conditions as internal reference.

Acknowledgements

This work was supported by the Consejo Nacional de Investigaciones Científicas y Técnicas (CONICET, Argentina) (Grant No. PIP 0370), Agencia Nacional de Promoción Científica y Tecnológica (ANPCyT, Argentina; PICT-2013-0905 and PICT-2016-1680), the Austrian Institute of Technology GmbH (AIT-CONICET Partner Group: "Exploratory Research for Advanced Technologies in Supramolecular Materials Science", Exp. 4947/11, Res. No. 3911, 28-12-2011), and Universidad Nacional de La Plata (UNLP). M.L.C., W.A.M, M.T. and O. A. are staff members of CONICET. M.L.A and S.E.H. gratefully acknowledge CONICET for their postdoctoral fellowships.

Conflict of interest

The authors declare no conflict of interest.

Keywords: colloids · crosslinking · PAH · phosphates · supramolecular chemistry

- [1] a) P. Davoodi, L. Y. Lee, Q. Xu, V. Sunil, Y. Sun, S. Soh, C.-H. Wang, *Adv. Drug Delivery Rev.* **2018**, *132*, 104–138; b) N. Bhattarai, J. Gunn, M. Zhang, *Adv. Drug Delivery Rev.* **2010**, *62*, 83–99; c) A. S. Hoffman, *Adv. Drug Delivery Rev.* **2012**, *64*, 18–23.
- [2] a) P. Calvo, C. Remuñán-López, J. L. Vila-Jato, M. J. Alonso, *J. Appl. Polym. Sci.* **1997**, *63*, 125–132; b) M. Rajanarivony, C. Vauthier, G. Couarraze, F. Puisieux, P. Couvreur, *J. Pharm. Sci.* **1993**, *82*, 912–917; c) U. K. De Silva, B. E. Weik, Y. Lapitsky, *Langmuir* **2014**, *30*, 8915–8922.
- [3] a) Z.-R. Lu, P. Qiao, *Mol. Pharm.* **2018**, *15*, 3603–3616; b) Z. Zhang, L. Shi, C. Wu, Y. Su, J. Qian, H. Deng, X. Zhu, *ACS Appl. Mater. Interfaces* **2017**, *9*, 29505–29514; c) T. M. Allen, P. R. Cullis, *Adv. Drug Delivery Rev.* **2013**, *65*, 36–48; d) V. P. Torchilin, *Nat. Rev. Drug Discovery* **2005**, *4*, 145–160.
- [4] a) M. Ferrari, *Nat. Rev. Cancer* **2005**, *5*, 161–171; b) M. E. Davis, Z. Chen, D. M. Shin, *Nat. Rev. Drug Discovery* **2008**, *7*, 771–782.
- [5] a) D. Hanahan, R. A. Weinberg, *Cell* **2000**, *100*, 57–70; b) M. G. Van der Heiden, L. C. Cantley, C. B. Thompson, *Science* **2009**, *324*, 1029–1033.
- [6] A. Schulze, A. L. Harris, *Nature* **2012**, *491*, 364–373.
- [7] a) J. R. Casey, S. Grinstein, J. Orłowski, *Nat. Rev. Mol. Cell Biol.* **2010**, *11*, 50–61; b) B. A. Webb, M. Chimenti, M. P. Jacobson, D. L. Barber, *Nat. Rev. Cancer* **2011**, *11*, 671–677.
- [8] a) Y. Lapitsky, *Curr. Opin. Colloid Interface Sci.* **2014**, *19*, 122–130; b) M. Chirea, C. M. Pereira, *F. Silva* **2007**, 1–6; c) K. E. Richardson, Z. Xue, Y. Huang, Y. Seo, Y. Lapitsky, *Carbohydr. Polym.* **2013**, *93*, 709–717.
- [9] a) V. S. Murthy, R. K. Rana, M. S. Wong, *J. Phys. Chem. B* **2006**, *110*, 25619–25627; b) W. A. Marmisollé, J. Irigoyen, D. Gregurec, S. Moya, O. Azzaroni, *Adv. Funct. Mater.* **2015**, *25*, 4144–4152.
- [10] N. Sawtarie, Y. Cai, Y. Lapitsky, *Colloids Surf. B* **2017**, *157*, 110–117.
- [11] H. Jonassen, A.-L. Kjøniksen, M. Hiorth, *Biomacromolecules* **2012**, *13*, 3747–3756.
- [12] a) Y. Cheng, S. Yu, X. Zhen, X. Wang, W. Wu, X. Jiang, *ACS Appl. Mater. Interfaces* **2012**, *4*, 5325–5332; b) J. Yu, M. A. Yaseen, B. Anvari, M. S. Wong, *Chem. Mater.* **2007**, *19*, 1277–1284.
- [13] a) H. G. Bagaria, M. S. Wong, *J. Mater. Chem.* **2011**, *21*, 9454–9466; b) P. Zhang, X. Song, W. Tong, C. Gao, *Macromol. Biosci.* **2014**, *14*, 1495–1504.

- [14] a) X. Z. Shu, K. J. Zhu, *Eur. J. Pharm. Biopharm.* **2002**, *54*, 235–243; b) P. Andreozzi, E. Diamanti, K. R. Py-Daniel, P. R. Cáceres-Vélez, C. Martinelli, N. Politakos, A. Escobar, M. Muzi-Falconi, R. Azevedo, S. E. Moya, *ACS Appl. Mater. Interfaces* **2017**, *9*, 38242–38254; c) F. T. Wall, J. W. Drenan, *J. Polym. Sci.* **1951**, *7*, 83–88.
- [15] a) G. Pérez-Mitta, W. A. Marmisollé, A. G. Albesa, M. E. Toimil-Molares, C. Trautmann, O. Azzaroni, *Small* **2018**, *14*, 1–8; b) K. Lutz, C. Gröger, M. Sumper, E. Brunner, *Phys. Chem. Chem. Phys.* **2005**, *7*, 2812–2815; c) N. E. Muzzio, M. A. Pasquale, W. A. Marmisollé, C. Von Bilderling, M. L. Cortez, L. I. Pietrasanta, O. Azzaroni, *Biomater. Sci.* **2018**, *6*, 2230–2247.
- [16] A. I. Petrov, A. A. Antipov, G. B. Sukhorukov, *Macromolecules* **2003**, *36*, 10079–10086.
- [17] H. Zhang, S. Mardiyani, W. C. W. Chan, E. Kumacheva, *Biomacromolecules* **2006**, *7*, 1568–1572.
- [18] R. K. Rana, V. S. Murthy, J. Yu, M. S. Wong, *Adv. Mater.* **2005**, *17*, 1145–1150.
- [19] Y. Xia, T. D. Nguyen, M. Yang, B. Lee, A. Santos, P. Podsiadlo, Z. Tang, S. C. Glotzer, N. A. Kotov, *Nat. Nanotechnol.* **2011**, *6*, 580–587.
- [20] M. Tagliazucchi, F. J. Williams, E. J. Calvo, *J. Phys. Chem. B* **2007**, *111*, 8105–8113.
- [21] H. Riegler, F. Essler, *Langmuir* **2002**, *18*, 6694–6698.
- [22] J. Choi, M. F. Rubner, *Macromolecules* **2005**, *38*, 116–124.
- [23] a) I. Borukhov, D. Andelman, R. Borrega, M. Cloitre, L. Leibler, *H. Orland*, **2000**, 11027–11034; b) M. Borkovec, G. J. M. Koper, *Macromolecules* **1997**, *30*, 2151–2158; c) D. Yoo, S. S. Shiratori, M. F. Rubner, *Macromolecules* **1998**, *31*, 4309–4318.
- [24] P. G. Lawrence, Y. Lapitzky, *Langmuir*. **2015**, *31*, 1564–1574.
- [25] M. Fang, *Chem. Mater.* **1999**, *11*, 1526–1532.
- [26] J. B. Schlenoff, *J. Chem. Phys.* **2018**, *149*, 163314.
- [27] H. Ochiai, Y. Anabuki, O. Kojima, K. Tominaga, I. Murakami, *J. Polym. Sci. Part B* **1990**, *28*, 233–240.
- [28] a) M. Tagliazucchi, I. Szleifer, *Soft Matter* **2012**, *8*, 7292; b) M. Ullner, B. Jönsson, *Macromolecules* **1996**, *29*, 6645–6655.

Manuscript received: January 14, 2019

Revised manuscript received: March 13, 2019

Version of record online: April 5, 2019